


Clock with 8×10^{-19} Systematic Uncertainty

Alexander Aepli^{1,*}, Kyungtae Kim¹, William Warfield¹, Marianna S. Safronova², and Jun Ye^{1,†}

¹*JILA, National Institute of Standards and Technology and the University of Colorado, Boulder, Colorado 80309-0440, USA and Department of Physics, University of Colorado, Boulder, Colorado 80309-0390, USA*

²*Department of Physics and Astronomy, University of Delaware, Newark, Delaware 19716, USA*

 (Received 14 March 2024; accepted 29 April 2024; published 10 July 2024)

We report an optical lattice clock with a total systematic uncertainty of 8.1×10^{-19} in fractional frequency units, representing the lowest uncertainty of any clock to date. The clock relies on interrogating the ultranarrow $^1S_0 \rightarrow ^3P_0$ transition in a dilute ensemble of fermionic strontium atoms trapped in a vertically-oriented, shallow, one-dimensional optical lattice. Using imaging spectroscopy, we previously demonstrated record high atomic coherence time and measurement precision enabled by precise control of collisional shifts and the lattice light shift. In this work, we revise the black body radiation shift correction by evaluating the $5s4d\ ^3D_1$ lifetime, necessitating precise characterization and control of many body effects in the $5s4d\ ^3D_1$ decay. Last, we measure the second order Zeeman coefficient on the least magnetically sensitive clock transition. All other systematic effects have uncertainties below 1×10^{-19} .

DOI: [10.1103/PhysRevLett.133.023401](https://doi.org/10.1103/PhysRevLett.133.023401)

Introduction.—Measuring time is one of the most fundamental tasks in physics, with each advancement in time-keeping enabling new discoveries and technologies [1,2]. Owing to the higher frequency of electronic transitions, the exceptional stability of optical metrology promises to revolutionize many disparate fields, from fundamental physics to navigation and geodesy. Over the past two decades, optical atomic clocks using neutral atoms or single ions have surpassed those based upon microwave transitions, setting records for both stability and accuracy [3–5]. Optical lattice clocks (OLCs) achieve ultrahigh stability by simultaneously interrogating many atoms tightly confined within a standing wave of light [6–8]. Every gain in stability and accuracy opens new realms of exploration, such as placing bounds on dark matter [9,10], probing general relativity [11,12], and will ultimately result in the redefinition of the Systeme International second [13–15].

Building upon two decades of optical lattice clock development, the JILA strontium 1D OLC utilizes a shallow lattice formed within an in-vacuum build up cavity first described in Ref. [16]. The $^{87}\text{Sr}\ ^1S_0 \rightarrow ^3P_0$ clock transition is addressed with a laser stabilized to a cryogenic, single-crystal silicon, optical resonator [17]. We previously reported record levels of atomic coherence and self-synchronous stability [16], cancellation of atomic interaction shifts [18], and precise control of the lattice light shift [19]. In this Letter, we report a complete systematic evaluation with a total uncertainty of 8.1×10^{-19} in fractional frequency units. Improved measurements of the second order Zeeman coefficient and the dynamic shift for black body radiation allow us to make significant strides in clock accuracy.

High accuracy operation.—To properly characterize and control systematic shifts, high measurement precision together with repeatable and reliable operation are key. Critical environmental control begins by stabilizing the air flow around the vacuum chamber to 20 °C with 100 mK peak-to-peak stability. Each viewport flange on the vacuum chamber is temperature stabilized via separate liquid loops with better than 20 mK stability. We directly measure the radiation temperature T and its stability at the atom's location by translating in a pair of calibrated in-vacuum temperature sensors [Fig. 1(a)].

An effusive oven generates a collimated beam of ^{87}Sr that is slowed and cooled using the broad $^1S_0 \rightarrow ^1P_1$ transition at 461 nm. The oven does not have direct line of sight to the main vacuum chamber, and we measure no temperature coupling to the oven at the atoms. This beam loads a magneto-optical trap (MOT) operating on this same transition. Further cooling on the $^1S_0 \rightarrow ^3P_1$ transition at 689 nm reduces the temperature to a few microkelvins [20]. This cooling light is stabilized to the same silicon resonator as the clock laser with hertz-level drift per day, making cooling robust over many months. As shown in Fig. 1(a), a magic wavelength optical lattice at 813 nm is formed within an in-vacuum buildup cavity oriented along gravity [16]. Atoms are loaded from the MOT into the lattice at a depth of 300 lattice photon recoil energies (E_r). Doppler cooling on the $^1S_0 \rightarrow ^3P_1\ F = 11/2$ transition reduces the radial temperature to ~ 700 nK, and resolved motional sideband cooling along the tightly confined direction \hat{Z} reduces the expected quantum state to $\langle n_Z \rangle < 0.05$. During Doppler and sideband cooling, we polarize the atomic sample in one of the $m_F = \pm 9/2$ stretched states.

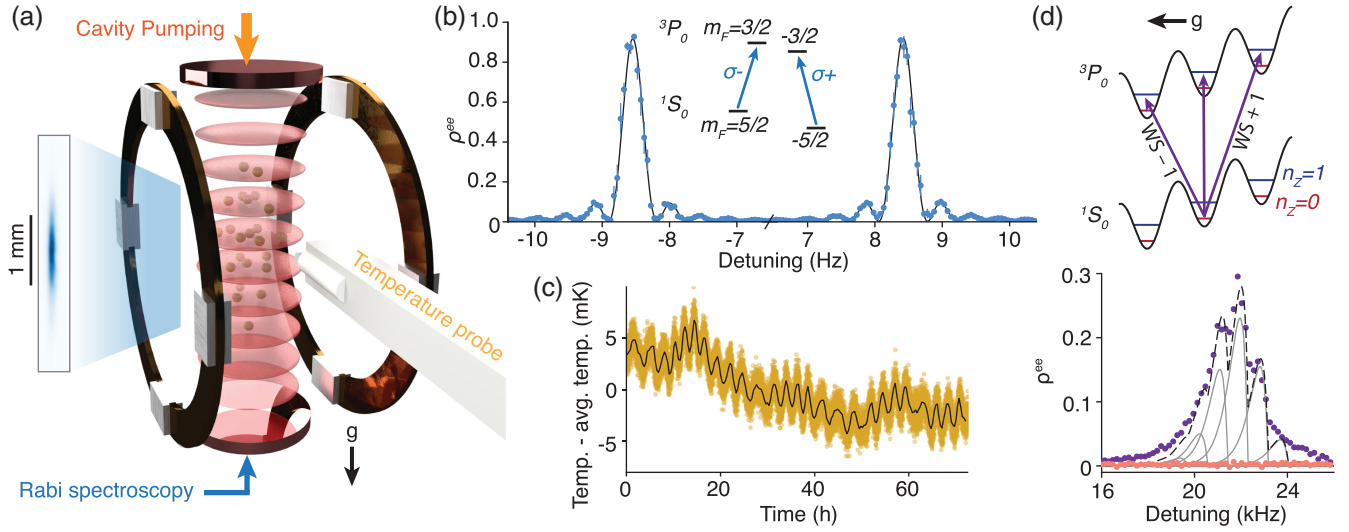


FIG. 1. Overview of the 1D optical lattice clock. (a) Schematic of the system highlights key aspects. Atoms are trapped in a 1D optical lattice formed within an in-vacuum buildup cavity oriented along the direction of gravity g . We read out the state of the atoms by imaging with a $6\ \mu\text{m}$ resolution. Rabi spectroscopy of the clock transition is performed along the tightly confined direction to remain within the resolved sideband regime. The two circular rings are quadrant electrodes for applying an electric field in any direction. A translatable temperature probe with two sensors measures the temperature. (b) 2.43 s Rabi spectroscopy of the two operational clock transitions. We prepare atoms in the $^1S_0, m_F = \pm 5/2$ states, drive the least magnetically sensitive clock transition to $^3P_0, m_F = \pm 3/2$, and measure the excitation fraction ρ^{ee} . Blue points are an average of five line scans with error bars given as the standard error. The black line is a Rabi line shape fit. (c) Temperature measured at the atom location over three days. The gold points are an average of the two sensors measured every ten seconds, and the black line is a 20 minute average. (d) Axial blue sideband (BSB) structure. The tilted, shallow lattice creates a set of site-changing Wannier-Stark (WS) transitions where the 3P_0 state occupies a different lattice site than the 1S_0 state. At our operational depth, only two motional states along the tight confinement direction exist, $n_z = 0$ and 1. In the lower panel, purple points show the $n_z = 0 \rightarrow 1$ transition. The structure of this spectrum is well captured by a model that incorporates the WS structure, the axial structure, and the radial temperature. Each gray line illustrates the BSB for each WS transition, with the sum of these in dashed black consistent with the data. In our standard clock sequence, the lattice depth is briefly reduced to $3 E_r$ before readout. The pink points near 0 demonstrate that this approach effectively eliminates all but the $n_z = 0$ population.

To reduce both the lattice light shift and the density shift, it is generally optimal to operate at a shallow lattice depth. Further, we identified a “magic lattice depth” near $15E_r$ where on-site interactions are canceled by off-site interactions, leading to a net-zero density shift [18]. Adiabatically ramping the lattice from the loading depth to $15E_r$ reduces the radial temperature to ~ 120 nK. The standard motional sideband model [21] is no longer reliable at these depths. The blue sideband, corresponding with adding one motional quanta along \hat{Z} , splits due to transitions to neighboring lattice sites as shown in Fig. 1(d). Thus it is necessary to use the lattice depth calibration technique introduced in Ref. [19].

To reduce the Zeeman effect sensitivity, we use the least magnetically sensitive $|^1S_0, m_F = \pm 5/2\rangle \rightarrow |^3P_0, m_F = \pm 3/2\rangle$ clock transition as illustrated in Fig. 1(b). Beginning with atoms in one of the stretched states, we apply two clock transfer pulses to prepare atoms in the $|^1S_0, m_F = \pm 5/2\rangle$ spectroscopy states with about 96% spin purity.

Between sample preparation and readout, the dead time is 1 s. Based upon a noise model of the clock laser, Dick noise is minimized with a 2.43 s Rabi interrogation

time [17]. A digital servo with two integrators tracks the atomic transition by alternating spin states and sides of the Rabi line shape. We expect a single clock stability of $5 \times 10^{-17}/\sqrt{\tau}$ for averaging time τ in seconds.

As shown in Fig. 1(d), we briefly reduce the lattice depth to the single band regime ($\sim 3 E_r$) before readout to ensure that the only measured atoms are in the $n_z = 0$ state. High resolution imaging to readout the clock excitation resolves spatial frequency variation [Fig. 1(a)], allowing for real-time density shift corrections. We operate with approximately 4×10^4 atoms, leading to a quantum projection noise of $< 3 \times 10^{-18}/\sqrt{\tau}$, which is near the self-synchronous comparison performance reported in Ref. [16].

Black body radiation shift.—The largest systematic shift in room temperature Sr clocks arises from the black body radiation (BBR) environment. The total differential BBR shift $\Delta\nu_{\text{BBR}}$ is the sum of a static component ν_{stat} that scales as T^4 , and a dynamic component ν_{dyn} that scales with higher powers of T . Thus, for accurate operation we need to determine T and the atomic response with high precision.

Radiation temperature: To ensure a fully thermal environment and measure the radiant temperature at the atoms, we follow a similar technique as in Refs. [4,22]. Two calibrated

thin film platinum resistance sensors are mounted to an in-vacuum translation arm, which is inserted into the middle of the vacuum chamber. During clock spectroscopy the probe is retracted 30 cm into an auxiliary vacuum chamber. We observe a submillikelvin temperature flicker floor at short timescales, ~ 2 mK peak oscillations on the hour timescale, and drift of less than a few millikelvin per day, as shown in Fig. 1(d). These few-hour temperature fluctuations are from coupling to room temperature and building process chilled water and can likely be improved by further system isolation. At 12 h the Allan deviation of the temperature is 1.4 mK, which we treat as the operational stability. The total temperature uncertainty is 4.1 mK [23].

ν_{dyn} evaluation: Accuracy in previous generations of room temperature Sr OLCs has been limited by the uncertainty in ν_{dyn} , which is directly tied to the $5s4d^3D_1$ lifetime [31]. As in Refs. [22,32], we prepare a sample of Sr atoms in 3P_0 before a $2.6 \mu\text{m}$ laser pulse excites a portion of the sample to the 3D_1 state. Some excited atoms decay to 3P_1 and then to the 1S_0 ground state, releasing a 689 nm photon in the process, as shown in Fig. 2(a). We collect this fluorescence with a cooled hybrid photomultiplier assembly (PMA) and time tag the incident photons with 5 ns resolution. In the single particle regime, the photon rate y at time t is well characterized by a cascaded double exponential process,

$$y(t) = A \times \Theta(t - t_0) \left(e^{-(t-t_0)/\tau_{3D_1}} - e^{-(t-t_0)/\tau_{3P_1}} \right) + y_0, \quad (1)$$

where A is the flux amplitude, Θ is a Heaviside function for instantaneous excitation at time t_0 , τ_{3D_1} and τ_{3P_1} are the 3D_1 and 3P_1 lifetimes, respectively, and y_0 is an offset due to background counts. In Fig. 2(b) we plot all collected photon counts and fit with Eq. (1). Since Eq. (1) assumes instantaneous excitation of atoms to 3D_1 , we do not fit data within a 500 ns window about the excitation pulse, indicated by the gray exclusion area [22].

At high densities in the 3P_0 state, we notice a modification to the exponential decay process. Spontaneous emission from one atom can affect the behavior of another atom, leading to effective dipole-dipole interactions and giving rise to effects like superradiance or radiation trapping. The interplay of these effects in this cascaded, multi-state decay is hard to simulate theoretically, and we do not have a complete model for extracting single particle lifetimes when such effects are present.

To use the model in Eq. (1) to determine the lifetime, it is vital to keep the population in 3P_0 low as it is the primary state that contributes to collective effects in the 3D_1 decay process. However, reducing atom number adversely affects averaging time. Instead, we load a large number of atoms in 1S_0 and promote a small portion of the atoms to 3P_0 . We then excite these atoms to 3D_1 with a 100 ns laser pulse. Since most of the atoms decay back to 3P_0 , we repeat this process 15 times before again exciting a portion of the 1S_0

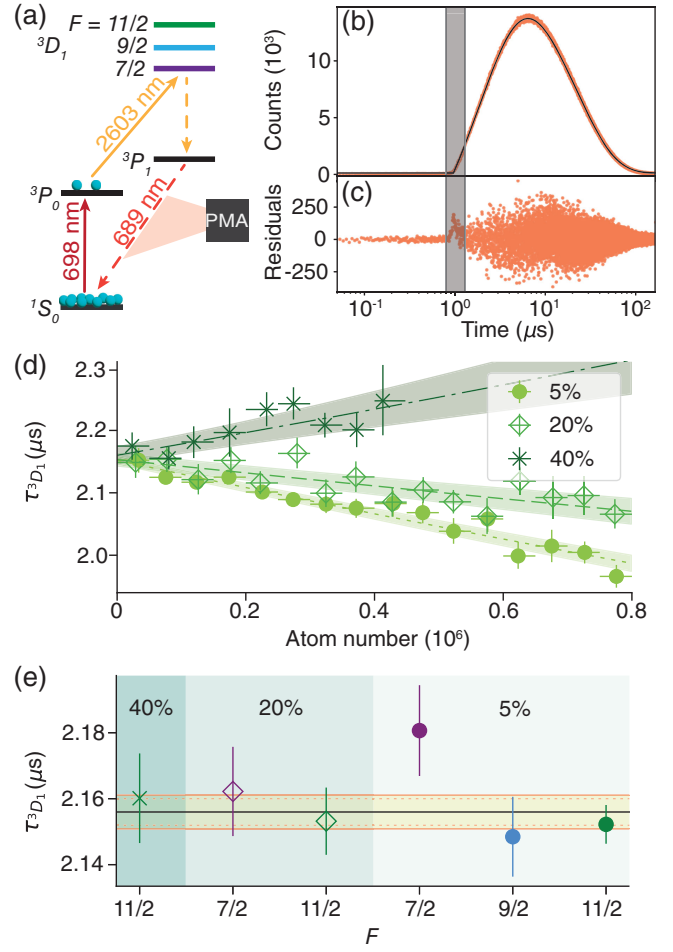


FIG. 2. $5s4d^3D_1$ lifetime measurement results. (a) Atoms are prepared in the 1S_0 ground state, a fraction are pumped to 3P_0 and then excited to one of the 3D_1 hyperfine levels F . Some of these atoms decay through 3P_1 back to 1S_0 , where we collect and time resolve the photons on a hybrid photomultiplier assembly (PMA). (b) Fit of Eq. (1) in black to all the collected data in orange. We exclude 500 ns window around the $2.6 \mu\text{m}$ excitation pulse, as shown in gray (c) Residuals of this fit. (d) The measured 3D_1 lifetime τ_{3D_1} as a function of total atom number for 3D_1 $F = 11/2$. The lines are density dependent lifetime fits with the shaded area showing the fit uncertainty. Varying the portion of the atoms in 3P_0 , shown as a percent of the total population, the density dependence of τ_{3D_1} changes. (e) Results of the six different data sets. Each point represents the zero density lifetime for different hyperfine levels F and 3P_0 population fractions, labeled above. The black line is the weighted average, the dashed lines show the statistical uncertainty, and the solid orange lines show the combined statistical and systematic uncertainty.

atoms to 3P_0 . After 10 clock pulses and a total of 150 3D_1 decay cycles, we Doppler cool the remaining sample. We repeat this excitation and cooling sequence 5 times before reloading a sample into the lattice. In sum, for each MOT sequence we collect photons from 750 decay cycles. On average we capture less than one photon from the sample per decay cycle, so pile-up effects are effectively eliminated.

Although the population that contributes to nonlinear collective effects is significantly reduced, weaker collective effects are still present. To understand how density affects the measured lifetime, we measure the total atom number at the beginning and end of the sequence and assign an atom number to each decay event.

Over the course of the measurement campaign, we collect 8×10^7 photons with a total atom number ranging from 10^3 to 10^6 . We collect data with different proportions of atoms in 3P_0 and iterate over all three hyperfine levels in 3D_1 , for a total of six separate data sets [23]. We divide each data set by atom number into bins with widths of 5×10^4 atoms and fit Eq. (1) to each bin. As in Ref. [32], we fit the lifetime density dependence $\tau(n) = \tau_0/(1 + cn)$, where n is the camera measured atom number and is proportional to density, τ_0 is the single atom lifetime, and c is the density dependence coefficient. At very high density, we notice that the data deviates from the linear model, so we choose to exclude data above 8×10^5 atoms in these fits. This choice does not change the final reported value. With small population in the 3P_0 state, the measured lifetime is shorter at higher density. However, by initially placing 40% of the population in 3P_0 the trend is reversed and higher density results in a longer observed lifetime, as shown for the $F = 11/2$ data in Fig. 2(d). The single atom lifetime for these six data sets is plotted in Fig. 2(e).

A number of other systematics can modify the measured lifetime. By applying a magnetic field (B) of ~ 1 G, we observe Zeeman beats due to interference between the emitted photons. We limit this effect by operating at zero field and periodically measure and correct the background $B < 2$ mG. A similar effect is caused by lattice light shifts splitting magnetic sublevels. To reduce this systematic, we measure the decay in a $10E_r$ lattice with the PMA oriented within a few degrees of the lattice light polarization. Modeling these effects we assign an uncertainty of 3 ns due to potential Zeeman beats. Using a weighted average of the six experimental conditions, we report $\tau_{^3D_1} = 2.156(5) \mu\text{s}$. This is plotted as the solid black line in Fig. 2(e), with the statistical uncertainty shown as the dashed orange lines and the total uncertainty as the solid orange lines.

This precisely determined 3D_1 lifetime allows us to re-evaluate ν_{dyn} based on the technique described in Ref. [33]. Using known atomic properties including measured transition strengths, magic wavelengths, and static polarizability, we determine $\nu_{\text{dyn}} = -153.06(33)$ mHz at 300 K [23]. The final BBR-related frequency shift combining both the static [34] and dynamic effects at the operational temperature of $20.132(4)^\circ\text{C}$ is $(-48417.2 \pm 7.3) \times 10^{-19}$.

Lattice light shift.—In previous work [19], we have demonstrated the ability to control the lattice light shift to a few parts in 10^{-19} . Because of the differential sensitivity to the lattice light shift of the motional states along the tightly confined direction, care must be taken to ensure repeatable

cooling of the sample in the lattice. The last stage of cooling is robust and stable, and we take a further step to reduce sample uncertainty by ramping the lattice to $3E_r$ before readout, ensuring that only the lowest band population is measured as shown in Fig. 1(d). With identical atomic coefficients as in Ref. [19], a lattice depth of $15.06(17) E_r$, and a 10.5 MHz lattice detuning from the measured operational magic frequency [35], the total light shift uncertainty is 3.2×10^{-19} .

dc Stark shift.—Stray electric fields can shift the clock transition frequency [36]. To limit the possibility of patch charges on the mirror surfaces causing these shifts, Faraday shields surround the mirrors and provide passive field attenuation. A pair of in-vacuum quadrant electrodes can apply electric fields in any direction across the atomic sample, shown as copper rings in Fig. 1(a). Alternating high and low fields, we precisely measure the residual dc Stark shift. The shift is below 10^{-21} along the cavity direction. The dominant source of residual field is along the imaging axis—likely due to patch charges on the large vacuum window nearby the atoms. The total residual dc Stark shift is $(-9.8 \pm 0.7) \times 10^{-20}$.

Zeeman shifts.—Because of the differential Landé- g factor [37] between the 1S_0 and 3P_0 states, we are sensitive to Zeeman shifts on the clock transition. Probing opposite spin states and taking the frequency average, we broadly reject this systematic. Yet there is still sensitivity to magnetic field fluctuations at and below the experiment cycle frequency. By using the $|^1S_0 m_F = \pm 5/2\rangle \rightarrow |^3P_0 m_F = \pm 3/2\rangle$ transition, we substantially reduce coupling to the magnetic environment, however even small field drifts may cause frequency shifts.

We use the 26 times more magnetically sensitive $|^1S_0 m_F = -5/2\rangle \rightarrow |^3P_0 m_F = -7/2\rangle$ transition to characterize this effect. Measuring this transition with the same duty cycle as in standard operation, the frequency difference between alternating cycles gives an upper bound on the first order Zeeman shift. We find a flicker floor of 0.78 mHz, leading to a total Zeeman shift uncertainty on the operational transition of 7×10^{-20} .

Operation on the $|^1S_0 m_F = \pm 5/2\rangle \rightarrow |^3P_0 m_F = \pm 3/2\rangle$ transition requires reevaluation of the second order Zeeman coefficient for our desired accuracy goal. This shift $\Delta\nu_{Z2}$ goes as

$$\Delta\nu_{Z2} = \xi_{\sigma m_F=5/2} (\Delta_{\text{meas}} - \Delta_{\text{vec}})^2, \quad (2)$$

where $\xi_{\sigma m_F=5/2}$ is the second order Zeeman coefficient, Δ_{meas} is the measured frequency difference between the operational transitions, and Δ_{vec} is the splitting due to the lattice vector shift.

To determine $\xi_{\sigma m_F=5/2}$ precisely, we vary the applied bias field from 0.3 to 1.5 G and measure the resultant frequency shift in an interleaved manner, as shown in Fig. 3. Δ_{vec} is measured independently by modulating the lattice depth.

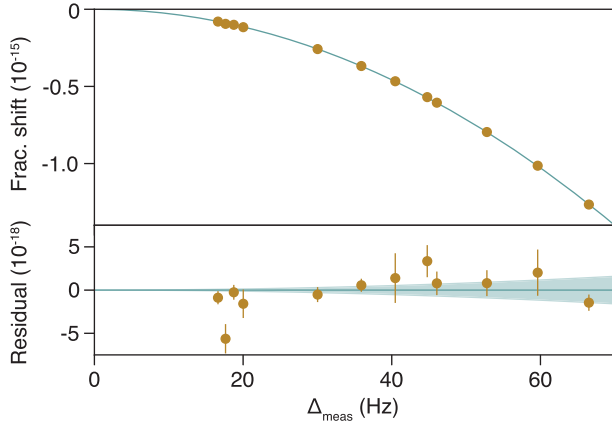


FIG. 3. Second order Zeeman shift coefficient measurement. We vary the applied magnetic field and measure the splitting (Δ_{meas}) and the frequency shift [see also Fig. 1(b)]. We fit the data with Eq. (2) and plot this fit in green. The lower panel shows the fit residuals with the shaded green region representing the fit uncertainty.

We find a $\xi_{\sigma_{m_F=5/2}} = -0.12263(14)$ mHz/Hz². At the operational field near 380 mG, the second order Zeeman shift $\Delta\nu_{ZZ} = (-85.51 \pm 0.10) \times 10^{-18}$.

Tunneling shift.—At shallow depths, superposition of states in neighboring sites can cause frequency shifts. First identified in Ref. [38], the maximum possible frequency shift due to this effect goes as $\Omega_0\Omega_1/\Delta_g$, where Ω_0 and Ω_1 are the Rabi frequencies of the carrier and first Wannier-Stark sideband and Δ_g is the frequency difference between neighboring lattice sites. At the operational depth of $15 E_r$, the off-site Rabi frequency is appreciably large, leading to a maximum shift of $\sim 2 \times 10^{-19}$. While the coherent superposition of neighboring states is likely small, it is difficult to directly measure and control this effect. Instead, we opt to use a Rabi pulse time that is a half integer multiple of the tunneling shift oscillation period [38]. We measure the splitting between neighboring lattice sites to be 867.7461(4) Hz. With a pulse time of 2.4298583 s and a conservative timing uncertainty of 1 μ s, the maximum tunneling shift is 2×10^{-21} .

Density shift.—Although strong collisional shifts are suppressed by the fermionic nature of ⁸⁷Sr, *p*-wave interactions lead to a systematic density shift [39,40]. Previous Sr OLCs required separate evaluation of collisional shifts, leading to drifting systematics as sample preparation varied over time [4]. With imaging synchronously measuring different densities and frequency shifts throughout the sample, we perform real-time density shift corrections. As reported in Ref. [18], operating at a magic lattice depth near $15 E_r$, on-site *p*-wave and off-site *s*-wave interactions cancel each other, substantially reducing the density shift even with a large atomic sample. For a single characteristic run ~ 300 min, the correction is $(-1.1 \pm 0.9) \times 10^{-19}$.

TABLE I. Fractional frequency shifts and uncertainties for the JILA 1D Sr optical lattice clock.

Shift name	Shift (10^{-19})	Uncertainty (10^{-19})
BBR	-48 417.2	7.3
Lattice light	-0.1	3.2
Second order Zeeman	-855.1	1.0
Density	-1.1	0.9
First order Zeeman	0.0	0.7
Background gas	-4.7	0.5
dc Stark	-1.0	0.1
Tunneling	0.0	<0.1
Minor shifts	0.0	<0.1
Total shift	-49 279.2	8.1

Other systematic shifts.—Collisions between trapped strontium atoms and background gas result in a systematic frequency shift [41]. In this system, the background gas is dominated by hydrogen molecules [23]. As demonstrated in [42], the shift is inversely proportional to the vacuum lifetime. Using this coefficient and a measured vacuum lifetime of 63.6 ± 2.5 s, we calculate a background gas shift of $(-4.7 \pm 0.5) \times 10^{-19}$.

Line pulling occurs if population in other magnetic sublevels is off-resonantly driven, distorting the carrier line shape. With a low intensity 2.43 s clock pulse, other transitions are highly suppressed. With 96% of the sample in the desired magnetic sublevel, we estimate for the worst case scenario a line pulling shift of $< 10^{-21}$.

Similarly, a low intensity Rabi drive significantly reduces the light shift from the clock laser. Using the coefficient measured in Ref. [43], and accounting for the increased intensity due to both light polarizations, we estimate the probe ac stark shift to be -4×10^{-22} , which we treat as the uncertainty.

Thermal transients in the acousto-optic modulator (AOM) due to switching may lead to an uncorrected Doppler shift. As in [4], we path length stabilize the same AOM order that drives the atomic transition. The AOM is ramped onto resonance after these thermal transients have settled, leading to an estimated probe chirp shift $< 10^{-21}$.

Summary.—Through precise atomic and environmental control, we have realized a strontium optical lattice clock with a total systematic accuracy of 8.1×10^{-19} as reported in Table I. This represents greater than a factor of 2 improvement in systematic accuracy over the previously most accurate strontium optical lattice clock [4], and it sets the accuracy benchmark of all optical clocks reported to date. Black body radiation stands out as the most significant source of uncertainty, and future cryogenic operation should reduce uncertainty to the low 10^{-19} level [44].

We thank S. Porsev for accurate atomic structure calculations, D. Wellnitz and A. M. Rey for useful discussions

on collective radiation effects, and C. Lisdat and U. Sterr for discussions about the dynamic BBR correction. We acknowledge contributions and discussions from the JILA Sr team, T. Bothwell, C. Kennedy, E. Oelker, J. Robinson, W. Tew, and A. Ellzey. We thank A. Chu and N. Darkwah Oppong for close reading of this manuscript. This research was supported in part through the use of University of Delaware HPC Caviness and DARWIN computing systems. Funding support is provided by NSF QLCI OMA-2016244, V. Bush Fellowship, the DOE Quantum Systems Accelerator, NIST, and NSF PHY-2317149. K. K. is supported in part by the Quantum Information Research Support Center funded by NRF Korea, MSIT-No. 2021M3H3A103657313.

*Alexander.Aeppli@colorado.edu

†Ye@jila.colorado.edu

- [1] National Academies of Sciences, Engineering, and Medicine, *Manipulating Quantum Systems: An Assessment of Atomic, Molecular, and Optical Physics in the United States* (The National Academies Press, Washington, DC, 2020).
- [2] A. D. Ludlow, M. M. Boyd, J. Ye, E. Peik, and P. O. Schmidt, Optical atomic clocks, *Rev. Mod. Phys.* **87**, 637 (2015).
- [3] W. F. McGrew, X. Zhang, R. J. Fasano, S. A. Schäffer, K. Beloy, D. Nicolodi, R. C. Brown, N. Hinkley, G. Milani, M. Schioppo, T. H. Yoon, and A. D. Ludlow, Atomic clock performance enabling geodesy below the centimetre level, *Nature (London)* **564**, 87 (2018).
- [4] T. Bothwell, D. Kedar, E. Oelker, J. M. Robinson, S. L. Bromley, W. L. Tew, J. Ye, and C. J. Kennedy, JILA SrI optical lattice clock with uncertainty of 2.0×10^{-18} , *Metrologia* **56**, 065004 (2019).
- [5] S. M. Brewer, J.-S. Chen, A. M. Hankin, E. R. Clements, C. W. Chou, D. J. Wineland, D. B. Hume, and D. R. Leibbrandt, $^{27}\text{Al}^+$ quantum-logic clock with a systematic uncertainty below 10^{-18} , *Phys. Rev. Lett.* **123**, 033201 (2019).
- [6] M. Takamoto, F.-L. Hong, R. Higashi, and H. Katori, An optical lattice clock, *Nature (London)* **435**, 321 (2005).
- [7] A. D. Ludlow, M. M. Boyd, T. Zelevinsky, S. M. Foreman, S. Blatt, M. Notcutt, T. Ido, and J. Ye, Systematic study of the ^{87}Sr clock transition in an optical lattice, *Phys. Rev. Lett.* **96**, 033003 (2006).
- [8] B. J. Bloom, T. L. Nicholson, J. R. Williams, S. L. Campbell, M. Bishof, X. Zhang, W. Zhang, S. L. Bromley, and J. Ye, An optical lattice clock with accuracy and stability at the 10¹⁸ level, *Nature (London)* **506**, 71 (2014).
- [9] M. Filzinger, S. Dörscher, R. Lange, J. Klose, M. Steinel, E. Benkler, E. Peik, C. Lisdat, and N. Huntemann, Improved limits on the coupling of ultralight bosonic dark matter to photons from optical atomic clock comparisons, *Phys. Rev. Lett.* **130**, 253001 (2023).
- [10] Boulder Atomic Clock Optical Network (BACON) Collaboration, Frequency ratio measurements at 18-digit accuracy using an optical clock network, *Nature (London)* **591**, 564 (2021).
- [11] M. Takamoto, I. Ushijima, N. Ohmae, T. Yahagi, K. Kokado, H. Shinkai, and H. Katori, Test of general relativity by a pair of transportable optical lattice clocks, *Nat. Photonics* **14**, 411 (2020).
- [12] X. Zheng, J. Dolde, M. C. Cambria, H. M. Lim, and S. Kolkowitz, A lab-based test of the gravitational redshift with a miniature clock network, *Nat. Commun.* **14**, 4886 (2023).
- [13] N. Dimarcq *et al.*, Roadmap towards the redefinition of the second, *Metrologia* **61**, 012001 (2024).
- [14] F. Riehle, Towards a redefinition of the second based on optical atomic clocks, *C.R. Phys.* **16**, 506 (2015).
- [15] J. Lodewyck, On a definition of the SI second with a set of optical clock transitions, *Metrologia* **56**, 055009 (2019).
- [16] T. Bothwell, C. J. Kennedy, A. Aeppli, D. Kedar, J. M. Robinson, E. Oelker, A. Staron, and J. Ye, Resolving the gravitational redshift across a millimetre-scale atomic sample, *Nature (London)* **602**, 420 (2022).
- [17] E. Oelker, R. B. Hutson, C. J. Kennedy, L. Sonderhouse, T. Bothwell, A. Goban, D. Kedar, C. Sanner, J. M. Robinson, G. E. Marti, D. G. Matei, T. Legero, M. Giunta, R. Holzwarth, F. Riehle, U. Sterr, and J. Ye, Demonstration of 4.8×10^{-17} stability at 1 s for two independent optical clocks, *Nat. Photonics* **13**, 714 (2019).
- [18] A. Aeppli, A. Chu, T. Bothwell, C. J. Kennedy, D. Kedar, P. He, A. M. Rey, and Jun Ye, Hamiltonian engineering of spin-orbit coupled fermions in a Wannier-Stark optical lattice clock, *Sci. Adv.* **8**, eadc9242 (2022).
- [19] K. Kim, A. Aeppli, T. Bothwell, and J. Ye, Evaluation of lattice light shift at low 10^{-19} uncertainty for a shallow lattice Sr optical clock, *Phys. Rev. Lett.* **130**, 113203 (2023).
- [20] H. Katori, T. Ido, Y. Isoya, and M. Kuwata-Gonokami, Magneto-optical trapping and cooling of strontium atoms down to the photon recoil temperature, *Phys. Rev. Lett.* **82**, 1116 (1999).
- [21] S. Blatt, J. W. Thomsen, G. K. Campbell, A. D. Ludlow, M. D. Swallows, M. J. Martin, M. M. Boyd, and J. Ye, Rabi spectroscopy and excitation inhomogeneity in a one-dimensional optical lattice clock, *Phys. Rev. A* **80**, 052703 (2009).
- [22] T. Nicholson, S. Campbell, R. Hutson, G. Marti, B. Bloom, R. McNally, W. Zhang, M. Barrett, M. Safronova, G. Strouse, W. Tew, and J. Ye, Systematic evaluation of an atomic clock at 2×10^{-18} total uncertainty, *Nat. Commun.* **6**, 6896 (2015).
- [23] See Supplemental Material at <http://link.aps.org/supplemental/10.1103/PhysRevLett.133.023401>, which includes [24–30], for more information.
- [24] A. Asenjo-Garcia, H. J. Kimble, and D. E. Chang, Optical waveguiding by atomic entanglement in multilevel atom arrays, *Proc. Natl. Acad. Sci. U.S.A.* **116**, 25503 (2019).
- [25] D. A. Steck, *Quantum and Atom Optics* (2022), <https://atomoptics.uoregon.edu/~dsteck/teaching/quantum-optics/quantum-optics-notes.pdf>.
- [26] D. Filin (private communication).
- [27] W. L. Tew, T. L. Nicholson, and R. B. Huston, Calibration of thin-film platinum sensors for use in the JILA Sr II Clock, NIST Technical Report NISTIR 8046, [10.6028/NIST.IR.8046](https://www.nist.gov/pml/nist-ir-8046) (2015).

- [28] M. Yasuda, T. Kishimoto, M. Takamoto, and H. Katori, Photoassociation spectroscopy of Sr 88: Reconstruction of the wave function near the last node, *Phys. Rev. A* **73**, 011403(R) (2006).
- [29] A. Heinz, A. J. Park, N. Šantić, J. Trautmann, S. G. Porsev, M. S. Safronova, I. Bloch, and S. Blatt, State-dependent optical lattices for the strontium optical qubit, *Phys. Rev. Lett.* **124**, 203201 (2020).
- [30] M. Takamoto, H. Katori, S. I. Marmo, V. D. Ovsiannikov, and V. G. Pal'chikov, Prospects for optical clocks with a blue-detuned lattice, *Phys. Rev. Lett.* **102**, 063002 (2009).
- [31] M. S. Safronova, S. G. Porsev, U. I. Safronova, M. G. Kozlov, and C. W. Clark, Blackbody-radiation shift in the Sr optical atomic clock, *Phys. Rev. A* **87**, 012509 (2013).
- [32] K. Beloy, J. A. Sherman, N. D. Lemke, N. Hinkley, C. W. Oates, and A. D. Ludlow, Determination of the $5d6s\ ^3D_1$ state lifetime and blackbody-radiation clock shift in Yb, *Phys. Rev. A* **86**, 051404(R) (2012).
- [33] C. Lisdat, S. Dörscher, I. Nosske, and U. Sterr, Blackbody radiation shift in strontium lattice clocks revisited, *Phys. Rev. Res.* **3**, L042036 (2021).
- [34] T. Middelmann, S. Falke, C. Lisdat, and U. Sterr, High accuracy correction of blackbody radiation shift in an optical lattice clock, *Phys. Rev. Lett.* **109**, 263004 (2012).
- [35] I. Ushijima, M. Takamoto, and H. Katori, Operational magic intensity for Sr optical lattice clocks, *Phys. Rev. Lett.* **121**, 263202 (2018).
- [36] J. Lodewyck, M. Zawada, L. Lorini, M. Gurov, and P. Lemonde, Observation and cancellation of a perturbing dc stark shift in strontium optical lattice clocks, *IEEE Trans. Ultrason. Ferroelectr. Freq. Control* **59**, 411 (2012).
- [37] M. M. Boyd, T. Zelevinsky, A. D. Ludlow, S. Blatt, T. Zanon-Willette, S. M. Foreman, and J. Ye, Nuclear spin effects in optical lattice clocks, *Phys. Rev. A* **76**, 022510 (2007).
- [38] P. Lemonde and P. Wolf, Optical lattice clock with atoms confined in a shallow trap, *Phys. Rev. A* **72**, 033409 (2005).
- [39] M. D. Swallows, M. Bishof, Y. Lin, S. Blatt, M. J. Martin, A. M. Rey, and J. Ye, Suppression of collisional shifts in a strongly interacting lattice clock, *Science* **331**, 1043 (2011).
- [40] M. J. Martin, M. Bishof, M. D. Swallows, X. Zhang, C. Benko, J. von Stecher, A. V. Gorshkov, A. M. Rey, and J. Ye, A quantum many-body spin system in an optical lattice clock, *Science* **341**, 632 (2013).
- [41] K. Gibble, Scattering of cold-atom coherences by hot atoms: Frequency shifts from background-gas collisions, *Phys. Rev. Lett.* **110**, 180802 (2013).
- [42] B. X. R. Alves, Y. Foucault, G. Vallet, and J. Lodewyck, Background gas collision frequency shift on lattice-trapped strontium atoms, in *Proceedings of the 2019 Joint Conference of the IEEE International Frequency Control Symposium and European Frequency and Time Forum (EFTF/IFC)*, Orlando, FL (IEEE, New York, 2019), 10.1109/FCS.2019.8856042.
- [43] Q. Xu, X. Lu, J. Xia, Y. Wang, and H. Chang, Measuring the probe Stark shift by frequency modulation spectroscopy in an ^{87}Sr optical lattice clock, *Appl. Phys. Lett.* **119**, 101105 (2021).
- [44] I. Ushijima, M. Takamoto, M. Das, T. Ohkubo, and H. Katori, Cryogenic optical lattice clocks, *Nat. Photonics* **9**, 185 (2015).